

Modulation of energy spectrum and control of coherent microwave transmission at single-photon level by longitudinal field in a superconducting quantum circuit

Xueyi Guo(郭学仪), Hui Deng(邓辉), Hekang Li(李贺康), Pengtao Song(宋鹏涛), Zhan Wang(王战), Luhong Su(苏鹭红), Jie Li(李洁), Yirong Jin(金贻荣), Dongning Zheng(郑东宁)
Citation: Chin. Phys. B . 2018, 27(7): 074206. **doi:** 10.1088/1674-1056/27/7/074206

Journal homepage: http://cpb.iphy.ac.cn; http://iopscience.iop.org/cpb

What follows is a list of articles you may be interested in

Coherently induced grating in refractive index enhanced medium

Zhuan-Zhuan Liu(刘撰撰), Yu-Yuan Chen(陈煜远), Jia-Yu Yuan(原佳宇), Ren-Gang Wan(万仁刚)
Chin. Phys. B . 2017, 26(12): 124209. **doi:** 10.1088/1674-1056/26/12/124209

High quality electromagnetically induced transparency spectroscopy of ^{87}Rb in a buffer gas cell with a magnetic field

Hong Cheng(成红), Han-Mu Wang(王汉睦), Shan-Shan Zhang(张珊珊), Pei-Pei Xin(辛培培), Jun Luo(罗军), Hong-Ping Liu(刘红平)
Chin. Phys. B . 2017, 26(7): 074204. **doi:** 10.1088/1674-1056/26/7/074204

Phase-controlled coherent population trapping in superconducting quantum circuits

Cheng Guang-Ling, Wang Yi-Ping, Chen Ai-Xi
Chin. Phys. B . 2015, 24(4): 044204. **doi:** 10.1088/1674-1056/24/4/044204

Switching from positive to negative absorption with electromagnetically induced transparency in circuit quantum electrodynamics

Li Hai-Chao, Ge Guo-Qin
Chin. Phys. B . 2014, 23(5): 054206. **doi:** 10.1088/1674-1056/23/5/054206

A simple scheme to generate χ-type four-charge entangled states in circuit QED

Gao Gui-Long,Song Fu-Quan,Huang Shou-Sheng,Wang Hui,Yuan Xian-Zhang,Wang Ming-Feng,Jiang Nian-Quan
Chin. Phys. B . 2012, 21(4): 044209. **doi:** 10.1088/1674-1056/21/4/044209

Modulation of energy spectrum and control of coherent microwave transmission at single-photon level by longitudinal field in a superconducting quantum circuit*

Xueyi Guo(郭学仪)[1,2], Hui Deng(邓辉)[1], Hekang Li(李贺康)[1,2], Pengtao Song(宋鹏涛)[1,2], Zhan Wang(王战)[1,2], Luhong Su(苏鹭红)[1,2], Jie Li(李洁)[1], Yirong Jin(金贻荣)[1,†], and Dongning Zheng(郑东宁)[1,2,‡]

[1] *Institute of Physics, Chinese Academy of Sciences, Beijing* 100190, *China*
[2] *University of Chinese Academy of Sciences, Beijing* 100049, *China*

(Received 20 April 2018; revised manuscript received 7 May 2018; published online 25 June 2018)

We study the effect of longitudinally applied field modulation on a two-level system using superconducting quantum circuits. The presence of the modulation results in additional transitions and changes the magnitude of the resonance peak in the energy spectrum of the qubit. In particular, when the amplitude λ_z and the frequency ω_l of the modulation field meet certain conditions, the resonance peak of the qubit disappears. Using this effect, we further demonstrate that the longitudinal field modulation of the Xmon qubit coupled to a one-dimensional transmission line could be used to dynamically control the transmission of single-photon level coherent resonance microwave.

Keywords: longitudinal field modulation (LFM), superconducting quantum circuit, microwave photonics

PACS: 42.50.Gy, 85.25.Cp **DOI:** 10.1088/1674-1056/27/7/074206

1. Introduction

Superconducting circuits are promising candidates in realizing scalable quantum computing.[1] The quantum coherence properties of superconducting qubits have been improved significantly over the past decade with a five orders of magnitude increase in coherence time, owing to progress in the optimization of materials, device design, and fabrication process.[2] The steady effort on the issues of measurement technique and isolation of modes and infrared radiation has also contributed to the performance of superconducting circuits.

Superconducting qubits can be regarded as two-level systems and the study of their quantum behavior is essential. Quantum two-level systems have been extensively studied in-depth. The simplest situation is its evolution driven by a resonant transverse field. The stationary Hamiltonian of the two-level systems is $H_0 = \frac{\hbar\omega_0}{2}\sigma_z$, where $\hbar\omega_0$ is the energy level difference between the ground and excited states and σ_z is the Pauli matrix. When a weak resonant transverse field drive $\hbar\lambda_x\cos(\omega_0 t)\sigma_x$ ($\lambda_x \ll \omega_0$) is applied, the rotate-wave approximation (RWA) is valid and the two-level system will do the Rabi oscillation.[3] The RWA ignores the counter rotate part that should not be ignored when the drive is strong.[4] Compared to the situation of driving a two-level system with transverse field, the study on the effect of longitudinal field applied to a two-level system is relatively lacking in the literature. Frequently, one applies a longitudinal bias dc-field to modify the energy level of a qubit. Recently, the effect of simultaneously applying longitudinal time varying field modulation and transverse field drive to a two-level system has been studied both theoretically and experimentally.[5–15] In this case, the dynamics of the two-level system is not simply described by Rabi oscillation. In a particular case, it is found that if the amplitude and frequency of the longitudinal field modulation (LFM) field take a certain ratio, the Rabi oscillation would disappear due to the modification of the energy levels by the LFM.[10] By using this effect, it has been demonstrated that the coupling strength between a superconducting flux qubit and a co-planer waveguide resonator could be changed in a controlled manner.[16]

In this work, we explore the effect of LFM on a two-level system using a Xmon superconducting qubit device. In Section 2, we consider the situation of simultaneously applying LFM and transverse field drive, and experimentally measure the excitation spectra of the Xmon. The results are in agreement with the theoretical analysis. In Section 3, we investigate the microwave photon transmission behavior of a superconducting one-dimensional coplanar waveguide (CPW) transmission line coupled to a Xmon qubit that is driven by a LFM field. The propagating wave is scattered by the qubit and the transmission is LFM dependent. We demonstrate dynamical control of the transmission characteristic of single-photon level coherent microwave through LFM pulse.

*Project supported by the Ministry of Science and Technology of China (Grant Nos. 2014CB921401, 2017YFA0304300, 2014CB921202, and 2016YFA0300601), the National Natural Science Foundation of China (Grant No. 11674376), and the Strategic Priority Research Program of the Chinese Academy of Sciences (Grant No. XDB07010300).

†Corresponding author. E-mail: jyr-king@iphy.ac.cn
‡Corresponding author. E-mail: dzheng@iphy.ac.cn

© 2018 Chinese Physical Society and IOP Publishing Ltd

2. Sample fabrication and measurement set-up

Two samples were used in this work. The superconducting qubit is of Xmon type in both samples.[17] The energy gap of the qubit can be adjusted by an external flux bias. In the first one, a Xmon qubit is capacitively coupled to a $\lambda/4$ coplanar waveguide (CPW) resonator that is coupled to a CPW transmission line. In this sample, the qubit state is readout by the dispersive method via the $\lambda/4$ resonator. In the second sample, a Xmon qubit is directly coupled to a transmission line and the interaction between an artificial atom (i.e., the Xmon qubit) and photons transmitted in the transmission line can be investigated. The optical micrographs of the two samples are shown in Figs. 1(a) and 2(a), respectively.

The samples were fabricated using a process involving electron-beam-lithography (EBL) and double-angle evaporation. In brief, a 100 nm thick Al layer was firstly deposited on a 10 mm×10 mm sapphire substrate by means of electron-beam evaporation, followed by EBL and wet etching to produce large structures such as microwave coplanar-waveguide resonators/transmission lines, capacitors of Xmon qubit, and electric leads. The EPL resist used was ZEP520 and the wet etching process was carried out using aluminum etchant type A. In the next step, the Josephson junctions of qubits were fabricated using the double-angle evaporation process. In this step, the under cut structure was created using a PMMA-MMA double layer EBL resist following a process similar to that reported in Ref. [18]. During the evaporation, the bottom electrode was about 30 nm thick while the top electrode was about 100 nm thick with intermediate oxidation.

In the measurements, the sample was mounted in an aluminum alloy sample box which was fixed on the mixing chamber stage of a dilution refrigerator. The temperature of the mixing chamber was below 15 mK during measurements. The input microwave lines and qubit fast bias control lines were heavily attenuated. Lines for qubit dc bias control were filtered using filters (RLC ELECTRONICS F-10-200-R) that functioned as combination of low-pass filter and copper powder filter. A bias-tee was used to combine the dc bias and LFM produced by an arbitrary wave generator (AWG). The microwave output signal from the transmission line was amplified (≈ 39 dB) by a cryogenic HEMT amplifier mounted at the 4 K stage and a room temperature amplifier (≈ 38 dB) before being measured either by a home-built heterodyne acquisition system or a vector network analyzer. The measurement set-ups are schematically shown in Figs. 1(b) and 2(b).

3. Excitation spectra of Xmon with LFM

Consider a simple two-level system subject to simultaneous longitudinal field modulation and transverse field drive. The Hamiltonian can be expressed as

$$\begin{aligned}\hat{H}(t) &= H_0 + H_{\text{longitudinal}}(t) + H_{\text{transverse}}(t)\\ &= \hbar\frac{\omega_0}{2}\sigma_z + \hbar\frac{\lambda_z}{2}\cos(\omega_{\text{l}}t)\sigma_z + \hbar\lambda_x\cos(\omega_{\text{e}}t)\sigma_x. \quad (1)\end{aligned}$$

Here, H_0 is the stationary Hamiltonian of the qubit, $H_{\text{longitudinal}}(t)$ is the LFM term, and $H_{\text{transverse}}(t)$ is the transverse field drive. Note that this transverse field drive is not necessarily in resonance with the qubit, i.e., ω_{e} is not necessarily equal to ω_0.

To study the effect of LFM, we apply uniform transformation

$$\hat{U}(t) = \exp\left[\text{i}\left(\frac{\omega_0}{2}t + \frac{\lambda_z}{2\omega_{\text{l}}}\sin(\omega_{\text{l}}t)\right)\sigma_z\right] \quad (2)$$

to Eq. (1). Then the Hamiltonian becomes

$$\begin{aligned}\hat{H}_{\text{eff}} &= \hbar\lambda_x\cos(\omega_{\text{e}}t)\\ &\times\begin{pmatrix}0 & \sum_{n=-\infty}^{\infty}J_n\left[\frac{\lambda_z}{\omega_{\text{l}}}\right]\exp[-\text{i}(\omega_0+n\omega_{\text{l}})t]\\ \text{c.c.} & 0\end{pmatrix}, \quad (3)\end{aligned}$$

where $J_n[x]$ is the n-th Bessel function of the first kind. Here we use the relation

$$\exp\left[\text{i}\frac{\lambda_z}{\omega_{\text{l}}}\sin(\omega_{\text{l}}t)\right] = \sum_{n=-\infty}^{\infty}J_n\left[\frac{\lambda_z}{\omega_0}\right]\exp[\text{i}n\omega_{\text{l}}t]. \quad (4)$$

From Eq. (3), we can see that only terms that meet $\omega_{\text{e}} = \omega_0 + n\omega_{\text{l}}$ $(n = 0, \pm1, \pm2, \ldots)$ will be non-zero over a time average. Thus, in this case, the Hamiltonian is further simplified to

$$\hat{H}_{\text{eff}} \approx \frac{\hbar\lambda_x}{2}J_n\left[\frac{\lambda_z}{\omega_{\text{l}}}\right]\sigma_x. \quad (5)$$

Therefore, we obtain the effective Rabi frequency $\frac{\lambda_x}{2}J_n[\frac{\lambda_z}{\omega_{\text{l}}}]$ for transverse field drive at frequency $\omega_{\text{e}} = \omega_0 + n\omega_{\text{l}}$.

From Eq. (5), we can easily see that the system should show two features. At first, because n can be any arbitrary integer, there should be other transitions besides the original transition at 0. Secondly, equation (5) shows that the effective Rabi frequency depends on the modulation amplitude λ_z and frequency ω_{l} through the Bessel functions. It is known that the Bessel functions have zeros for certain values of arguments. Therefore, an important feature stemmed from Eq. (5) is that the effective Rabi frequency would become zero for certain ratio of $\lambda_z/\omega_{\text{l}}$. For instance, in the case of $n = 0$, $J_0[\frac{\lambda_z}{\omega_{\text{l}}}] = 0$ while $\frac{\lambda_z}{\omega_{\text{l}}} \approx 2.4$. Figure 1 illustrates the two processes with and without the LFM.

To verify the effective Rabi oscillations induced by the LFM at different amplitude and frequency, we performed excitation spectra measurements on a Xmon qubit by applying the continuous weak transverse field drive through XY control line and LFM through Z control line. Similar experiments were conducted in Ref. [15] for a superconducting transmon qubit. In the spectra measurements, the intensity of the corresponding transitions is proportional to the population that can be obtained from the density matrix.

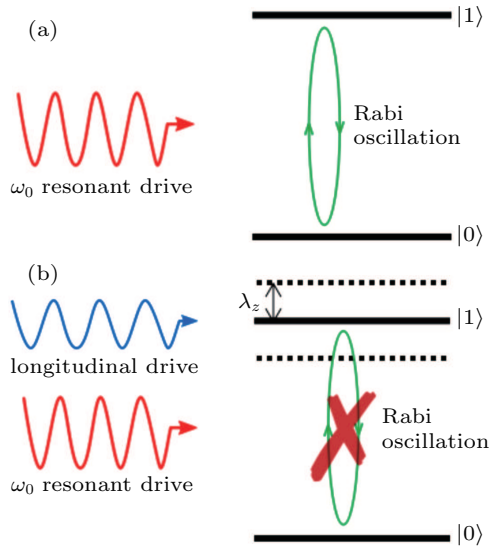


Fig. 1. (color online) (a) Schematic illustration of Rabi oscillation. (b) Schematic illustration for the disappearance of Rabi oscillation with LFM.

The time evolution of the density matrix of the system is described by the master equation

$$\frac{\mathrm{d}\rho}{\mathrm{d}t} = -\frac{\mathrm{i}}{\hbar}[\hat{H}_{\mathrm{eff}}, \rho] + \hat{L}[\rho], \tag{6}$$

where $\hat{L}$ is the Lindblad operator that accounts for the energy relaxation and dephasing process of the system. The final equilibrium population of $|1\rangle$, i.e. ρ_{11}, is related to $\hat{H}_{\mathrm{eff}}$ in Eq. (5), and thus

$$\rho_{11} \propto \left| \frac{\hbar\lambda_x}{2} J_n\left[\frac{\lambda_z}{\omega_1}\right] \right|. \tag{7}$$

We first measured the basic characteristic parameters of the samples. For the first sample, the maximum frequency of the Xmon qubit is $\omega_{01}^{\mathrm{MAX}}/2\pi = 6.984$ GHz and its anharmonicity $(\omega_{12} - \omega_{01})/2\pi = -215$ MHz. Here, we label the lowest three levels of Xmon as $|0\rangle$, $|1\rangle$, and $|2\rangle$. The resonator frequency would shift according to the qubit state when they are dispersively coupled to each other. Thus, for the maximum qubit frequency bias point, the resonator frequency becomes $\omega_{\mathrm{r},|0\rangle}/2\pi = 6.5564$ GHz and $\omega_{\mathrm{r},|1\rangle}/2\pi = 6.5542$ GHz when Xmon is at $|0\rangle$ state and $|1\rangle$ state, respectively. The coupling strength between the Xmon and the readout resonator is $g = \sqrt{-\chi\Delta(1+\Delta/\eta)} \approx 36$ MHz, where $\Delta \equiv \omega_{01} - \omega_{\mathrm{r}}$ and $\eta \equiv \omega_{12} - \omega_{01}$. Finally, by performing time domain measurements, we obtained the qubit energy relaxation time $T_1 = 5.27$ μs.

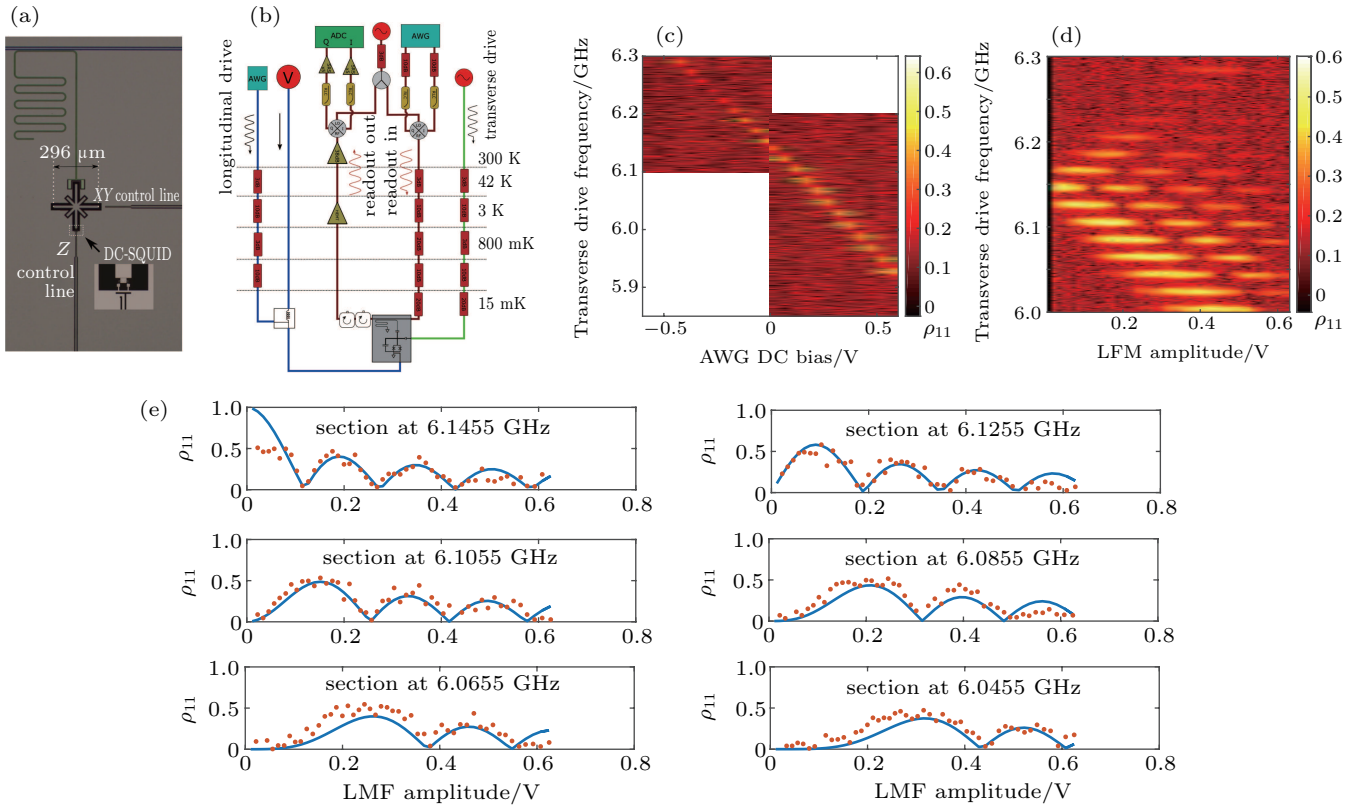


Fig. 2. (color online) (a) Optical micrograph of the Xmon qubit of the first sample. The green part is a $\lambda/4$ CPW resonator for readout. The red cross part is the capacitor of Xmon and the inset shows the DC-SQUID of Xmon which works as an adjustable non-linear inductance. The *XY* control line is used to apply a transverse field drive and the *Z* control line is used to apply the bias field and thus to apply LFM. (b) Schematic diagram of measurement setup. (c) Energy spectra of the Xmon qubit measured as a function of bias voltages. (d) Xmon qubit energy spectra variation with LFM amplitude. The qubit is biased at $\Phi = 0.15758\Phi_0$, corresponding to an energy difference $\omega_0 = 6.1455$ GHz and the LFM frequency is fixed at 20 MHz. (e) Resonate peak intensity as a function of LFM amplitude for 6 branches (corresponding to $n = 0, -1, \ldots, -5$) shown in (d). The solid lines are fitting of the Bessel function (Eq. (5)) to the experimental data.

In Fig. 2(c), we show a part of the energy spectra of the Xmon qubit as a function of dc bias. For the Xmon qubit, the energy difference between the ground state and the first excited state is $\hbar\omega_{01}(\phi) \approx \sqrt{8E_{\rm J}(t)E_{\rm c}} - E_{\rm c}$, where $E_{\rm J}$ and $E_{\rm c}$ represent the junction energy and charge energy, respectively. $E_{\rm J}$ can be adjusted by external flux Φ via the relation $E_{\rm J}(t) = E_{\rm J,max}|\cos(\pi\Phi(t)/\Phi_0)|$. Because ω_{01} is insensitive to Φ at the maximum frequency point, we bias the qubit to a point $\Phi = 0.15758\Phi_0$ with dc-bias. The correspoing qubit frequency is $\omega_0 = \omega_{01} = 2\pi \cdot 6.1455$ GHz.

The dependence of the Xmon qubit energy level difference on the external flux is not linear. Therefore, in order to obtain a sinusoidal modulation, we need to calibrate the output voltage waveform of the AWG used in our measurements. This can be easily done with the AWG according to the above mentioned relations among $\hbar\omega_{01}$, $E_{\rm J}$, and Φ.

We measured the excitation spectra with a fixed LFM frequency of 20 MHz and investigated its variation with LFM amplitude. The experiment results are shown in Fig. 2(d). Clearly, as would be expected from Eqs. (2) and (3), additional resonate transition peaks appear. The frequency difference between the neighbor peaks is $\omega_{\rm l} = 20$ MHz. It also shows that at certain LMF voltages, the resonate peaks disappear, as would be expected from Eq. (5). In Fig. 2(e), we present the resonate peak intensity as a function of LFM amplitude for 6 branches (corresponding to $n = 0, -1, \ldots, -5$) shown in Fig. 2(d). The solid lines are fitting of the Bessel function (Eq. (5)) to the experimental data. The measured result is in good agreement with the theoretical analysis.

We note that in Fig. 2(d), the excitation peak intensity is weaker in the upper branches than that in the lower ones. We attribute this to the variation of energy relaxation time T_1 at different bias points. The data shown in Fig. 2(c) appear to support this explanation with relatively weak excitation peaks at the high frequency region.

4. Control of transmission of single-photon level coherent microwave by LFM

In the previous section, we showed LFM induced transparency with Xmon excitation spectra. In this section, we coupled a Xmon in a one-dimensional transmission line to study the related quantum optic effect when applying LFM to Xmon.

The effect of superconducting artificial atom on the transmission coherent microwave photons has been reported in Refs. [19] and [20]. For example, strong atom–field interaction was realized with a superconducting flux qubit embedded in a one-dimensional transmission line, demonstrating a high degree extinction of propagating wave and showing the resonance fluorescence.[19] Later in another work, a transmon qubit was embedded in a one-dimensional transmission line, and the authors used the ATS effect to control the passage or reflection of single-photon level coherent microwave.[20] Other quantum optical effects and applications due to the interaction between artificial atoms and propagating photons in one-dimension transmission lines were studied theoretically and experimentally in Refs. [21]–[37].

In the following, we show that the LFM on a qubit can change the transmission properties of single-photon level coherent microwave. As shown in Ref. [19], for a qubit placed at $x = 0$ and an incident microwave $V_0(x,t) = V_0\,{\rm e}^{{\rm i}kx - {\rm i}\omega_0 t}$, where k is the wavenumber and ω_0 is the frequency, if the qubit frequency also is ω_0, the scattered wave is $V_{\rm sc}(x,t) = V_{\rm sc}\,{\rm e}^{{\rm i}k|x| - {\rm i}\omega_0 t}$. Then, the reflected wave is $V_{\rm r}(x,t) = V_{\rm sc}$, and the transmitted wave is the coherent interference of the scattered wave and incident wave $V_{\rm t}(x,t) = V_0 + V_{\rm sc}$. Because of the boundary condition for the scattered wave, the scattered wave is in opposite phase with the incident wave. Hence, these two waves are in destruction interference in the transmitted direction.

If the qubit is modulated by LFM, the energy level difference becomes $\hbar(\omega_0 + \lambda_z\cos(\omega_{\rm l}t))$. It would generate scattered waves with multiple frequency, and the amplitude of each different frequency component varies in the form $J_n[\frac{\lambda_z}{\omega_{\rm l}}]$. This may be understood with the following formula:

$$\begin{aligned} V_{\rm sc}(x,t) &= V_{\rm sc}\,{\rm e}^{{\rm i}k|x| - {\rm i}\omega_0 t - {\rm i}\frac{\lambda_z}{\omega_{\rm l}}\sin(\omega_{\rm l}t)} \\ &= V_{\rm sc}\,{\rm e}^{{\rm i}k|x| - {\rm i}\omega_0 t}\sum_{n=-\infty}^{\infty} J_n\left[\frac{\lambda_z}{\omega_{\rm l}}\right]{\rm e}^{-{\rm i}n\omega_{\rm l}t} \\ &= \sum_{n=-\infty}^{\infty} V_{\rm sc}J_n\left[\frac{\lambda_z}{\omega_{\rm l}}\right]{\rm e}^{{\rm i}k|x| - {\rm i}(\omega_0 + n\omega_{\rm l})t}. \end{aligned} \tag{8}$$

Thus, in the transmitted direction, when the incident wave frequency equals to $\omega_0 + n\omega_{\rm l}$ $(n = 0, \pm1, \pm2, \ldots)$, it also will be in destruction interference with the scattered wave, and the net wave amplitude is affected by the scattered wave amplitude. Supposing the frequency of incident wave $\omega_i = \omega_0 + n\omega_{\rm l}$ and using the opposite phase condition, we obtain the transmission coefficient

$$\begin{aligned} |S_{21}| &= \frac{|V_0 + V_{\rm sc}|}{|V_0|} \\ &= \frac{|V_0\,{\rm e}^{{\rm i}kx - {\rm i}\omega_i t} - V_{\rm sc}|J_n[\frac{\lambda_z}{\omega_{\rm l}}]|\,{\rm e}^{{\rm i}k|x| - {\rm i}(\omega_0 + n\omega_{\rm l})t}|}{|V_0|} \\ &= \frac{|V_0 - V_{\rm sc}|J_n[\frac{\lambda_z}{\omega_{\rm l}}]||}{|V_0|}. \end{aligned} \tag{9}$$

In experiment, we can measure how S_{21} change with the LFM amplitude.

The measured data are shown in Fig. 3. The energy spectra of the Xmon qubit as a function of dc-bias voltage are displayed in Fig. 3(d). To study the effect of LFM, the qubit is tuned at 5.779 GHz while a LFM with a fixed frequency 50 MHz is applied to the qubit via the Z control line. Again, the AWG output waveform is calibrated for producing LFM using the method mentioned in the previous section.

The transmission spectra of the sample measured at different frequencies as a function of LFM amplitude are shown in Fig. 3(e). Clearly, the results are in agreement with Eq. (9) and show that the transmission can be modulated by LFM. According to Eq. (9), the transmission coefficient becomes unit when $J_n[\frac{\lambda_z}{\omega_l}]$ is zero. Thus, we may choose appropriate λ_z and ω_l to obtain full transparency of the incident microwave waves at a frequency in resonant with the qubit.

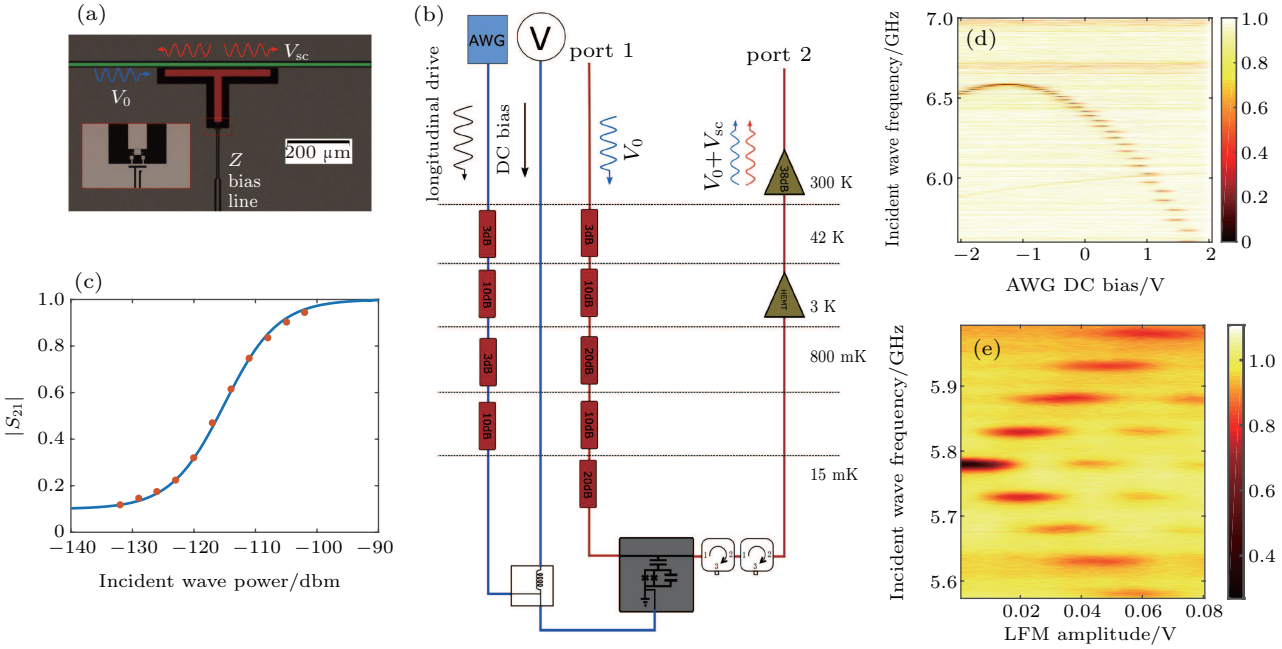


Fig. 3. (color online) (a) Optical micrograph of the second sample. The green part is a one-dimensional open transmission line. The red part is the Xmon and the inset is the dc-SQUID of Xmon. LFM can be applied through Z control line. (b) Schematic diagram of experiment setup for transmission spectrum measurement. The incident microwave is fed in through port 1 and the output signal is picked up on port 2. LFM is generated by an AWG and the dc bias is generated by a dc voltage source. These two bias signals are combined by a bias-tee and connect to the Z control line. (c) Transmission coefficient S_{21} as a function of incident microwave power at the frequency in resonant with the Xmon qubit. In this case, the frequency is 6.42793 GHz. The red dot is the experiment data, and the blue solid line is the fitting curve of Eq. (**??**). (d) Qubit energy spectra variation with dc bias obtained from S_{21} measurements without LFM. (e) Qubit energy spectra at a fixed dc-bias, corresponding to a qubit frequency 5.779 GHz, measured from S_{21} measurements with LFM. The LFM frequency is 50 MHz and the amplitude is varied.

In the following, we demonstrate transient control of single-photon level coherent microwave transmission by turning on and off the LFM. At first, we measure the transmittance as a function of the incident wave power and the results are shown in Fig. 3(c). Transmission behaviors of such kinds of samples have been studied in Refs. [19] and [20]. If the incident wave is in resonant with the qubit, its transmission coefficient is

$$t = |S_{21}| = 1 - r_0 \frac{1}{1 + \Omega^2/\Gamma_1\Gamma_2}, \tag{10}$$

where $r_0 = \eta/(1 + 2\Gamma_\phi/\Gamma_1)$. η is a dimensionless coupling efficiency of Xmon and transmission line, and Γ_1 is the energy relaxation rate of Xmon from $|1\rangle$ to $|0\rangle$. $\Gamma_2 = \Gamma_1/2 + \Gamma_\phi$ is the dephasing rate and Γ_ϕ is the pure dephasing rate. Ω is the Rabi frequency of Xmon and $\Omega \propto |V_0|$. The solid line in Fig. 3(c) represents the fitting of the experimental data to Eq. (10). We define an average number of photons per interaction time $2\pi/\Gamma_1$ as $\langle n\rangle \equiv 2\pi P/(\hbar\omega_0\Gamma_1)$. At a low incident microwave power (≈ -130 dBm and $\langle n\rangle \approx 2$ calculated with $\Gamma_1 \approx 2\pi \cdot 10$ MHz), we measured the transmission coefficient with LFM being turned on and off.

According to the data in Fig. 3(e), we determine that for the 50 MHz LFM, the transparency appears at $\omega_0 =$ 5.779 GHz when the amplitude of LFM waveform output by the AWG is about 0.027 V. The data are shown in Fig. 4 in which a LFM pulse of 1 μs is applied. Clearly, we observe the modulation of the transmission by LFM. We would like to point out that this is an alternative approach as compared to the previously reported method of using the ATS effect[20] or direct detuning the 0–1 transition frequency. It may find applications in building quantum networks. We note that there is still about 20% transmission when the LFM is turned off. We believe that this could be improved by increasing the coupling strength between the Xmon qubit and the transmission line.

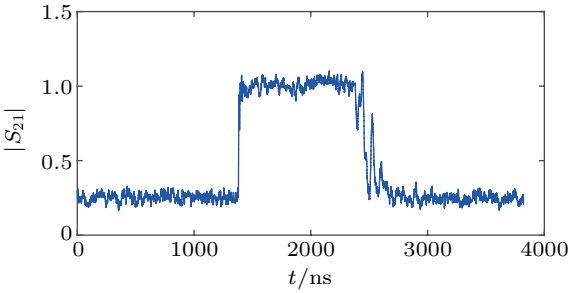


Fig. 4. (color online) Dynamic control of the transmittance of single-photon level coherent microwave with LFM pulse. Incident microwave is at frequency 5.779 GHz. We apply a calibrated 1 μs LFM pulse and measure the response of S_{21}. When the LFM is applied, the microwave is totally transmitted. Without LFM, the microwave is 80% reflected.

5. Conclusion

We have investigated the effect of longitudinal field modulation on the properties of superconducting Xmon qubit. In the first experiment, we measured the excitation spectra of a superconducting Xmon qubit while simultaneously applying a longitudinal field modulation through the Z control line and a transverse field drive through the XY control line. We observed the appearance of transitions at frequencies different from the qubit frequency by multiple times of the modulation frequency. Furthermore, transition peaks disappeared when the amplitude λ_z and frequency ω_l of the modulation field met the condition $\lambda_z \approx 2.4\omega_l$, as if the qubit became transparent to the resonance photons. In the second experiment, we used this effect to dynamically control the transmission of coherent microwave at the single-photon level.

References

[1] Devoret M H and Schoelkopf R J 2013 *Science* **339** 1169
[2] Oliver William D and Welander Paul B 2013 *MRS Bulletin* **38** 816
[3] Rabi I I, Ramsey N F and Schwinger J 1954 *Rev. Mod. Phys.* **26** 167
[4] Wu Ying and Xiaoxue Yang 2007 *Phys. Rev. Lett.* **98** 013601
[5] Lü Z and Zheng H 2012 *Phys. Rev. A* **86** 023831
[6] Yan Y, Lü Z and Zheng H 2014 *Phys. Rev. A* **90** 053850
[7] Lü Z, Yan Y, Goan H S and Zheng H 2016 *Phys. Rev. A* **93** 033803
[8] Yan Y, Lü Z, Zheng H and Zhao Y 2016 *Phys. Rev. A* **93** 033812
[9] Yan Y, Lü Z, Luo J and Zheng H 2017 *Phys. Rev. A* **96** 033802
[10] Liu Y X, Yang C X, Sun H C and Wang X B 2014 *New J. Phys.* **16** 015031
[11] Silveri M, Tuorila J, Kemppainen M and Thuneberg E 2013 *Phys. Rev. B* **87** 134505
[12] Nakamura Y, Pashkin Y A and Tsai J S 2001 *Phys. Rev. Lett.* **87** 246601
[13] Wilson C M, Duty T, Persson F, Sandberg M, Johansson G and Delsing P 2007 *Phys. Rev. Lett.* **98** 257003
[14] Wilson C M, Johansson G, Duty T, Persson F, Sandberg M and Delsing P 2010 *Phys. Rev. B* **81** 024520
[15] Li J, Silveri M, Kumar K, Pirkkalainen J M, Vepsäläinen A, ChienW, Tuorila J, Sillanpää M, Hakonen P, Thuneberg E and Paraoanu G 2013 *Nat. Commun.* **4** 1420
[16] Wu Y, Yang L P, Zheng Y, Deng H, Yan Z, Zhao Y, Huang K, Munro W J, Nemoto K, Zheng D N, Sun C P, Liu Y X, Zhu X and Lu L 2016 arXiv:1605.06747 [quant-ph]
[17] Barends R, Kelly J, Megrant A, Sank D, Jeffrey E, Chen Y, Yin Y, Chiaro B, Mutus J, Neill C, O'Malley P, Roushan P, Wenner J, White T C, Cleland A N and Martinis J M 2013 *Phys. Rev. Lett.* **111** 080502
[18] Kelly J S 2015 *Fault-tolerant Superconducting Qubits* (Ph.D. Dissertation) (Santa Barbara: University of California)
[19] Astafiev O, Zagoskin A M, Abdumalikov A A, Pashkin Y A, Yamamoto T, Inomata K, Nakamura Y and Tsai J S 2010 *Science* **327** 840
[20] Hoi I C, Wilson C M, Johansson G, Palomaki T, Peropadre B and Delsing P 2011 *Phys. Rev. Lett.* **107** 073601
[21] Shen J T and Fan S 2005 *Phys. Rev. Lett.* **95** 213001
[22] Abdumalikov A A, Astafiev O, Zagoskin A M, Pashkin Y A, Nakamura Y and Tsai J S 2010 *Phys. Rev. Lett.* **104** 193601
[23] Astafiev O V, Abdumalikov Jr A A, Zagoskin A M, Pashkin Y A, Nakamura Y and Tsai J S 2010 *Phys. Rev. Lett.* **104** 183603
[24] Abdumalikov A A, Astafiev O V, Pashkin Y A, Nakamura Y and Tsai J S 2011 *Phys. Rev. Lett.* **107** 043604
[25] Wilson C M, Johansson G, Pourkabirian A, Simoen M, Johansson J R, Duty T, Nori F and Delsing P 2011 *Nature* **479** 376
[26] Hoi I C, Palomaki T, Lindkvist J, Johansson G, Delsing P and Wilson C M 2012 *Phys. Rev. Lett.* **108** 263601
[27] Hoi I C, Kockum A F, Palomaki T, Stace T M, Fan B, Tornberg L, Sathyamoorthy S R, Johansson G, Delsing P andWilson C M 2013 *Phys. Rev. Lett.* **111** 053601
[28] Hoi I C, Wilson C M, Johansson G, Lindkvist J, Peropadre B, Palomaki T and Delsing P 2013 *New J. Phys.* **15** 025011
[29] Koshino K, Terai H, Inomata K, Yamamoto T, Qiu W, Wang Z and Nakamura Y 2013 *Phys. Rev. Lett.* **110** 263601
[30] Koshino K, Inomata K, Yamamoto T and Nakamura Y 2013 *Phys. Rev. Lett.* **111** 153601
[31] Loo A F V, Fedorov A, Lalumi.ere K, Sanders B C, Blais A and Wallraff A 2013 *Science* **342** 1494
[32] Inomata K, Koshino K, Lin Z R, Oliver W D, Tsai J S, Nakamura Y and Yamamoto T 2014 *Phys. Rev. Lett.* **113** 063604
[33] Mlynek J A, Abdumalikov A A, Eichler C and Wallraff A 2014 *Nat. Commun.* **5** 5186
[34] Hoi I C, Kockum A F, Tornberg L, Pourkabirian A, Johansson G, Delsing P and Wilson C M 2015 *Nat. Phys.* **11** 1045
[35] Inomata K, Lin Z, Koshino K, Oliver W D, Tsai J S, Yamamoto T and Nakamura Y 2016 *Nat. Commun.* **7** 12303
[36] Forn-Díaz P, García-Ripoll J J, Peropadre B, Orgiazzi J L, Yurtalan M A, Belyansky R, Wilson C M and Lupascu A 2017 *Nat. Phys.* **13** 39
[37] Liu Y and Houck A A 2017 *Nat. Phys.* **13** 48